Field PMU Test and Calibration Method—Part II: Test Signal Identification Methods and Field Test Applications

Sudi Xu, Hao Liu, and Tianshu Bi

***Abstract*—Synchrophasor measurement units (PMUs) provide synchronized measurement data for wide-area applications. To improve the effectiveness of synchrophasor-based applications, field PMUs must be tested to ensure their performance and data quality. In the companion paper (Part I), we proposed a field PMU test and calibration framework consisting of a PMU calibrator and analysis center. Part I presents the development and test of the PMU calibrator. This paper focuses on the analysis center and field test applications. First, the critical component of the analysis center is the signal identification module, for which the step and oscillation signal identification methods are proposed. Here, the performance evaluation criteria of PMU in these two cases are different from others. The methods include a step signal detection method based on singular value decomposition (SVD), which has the capability of weak step detection to account for energy leakage of the signal during the step process, and an oscillation signal identification method based on SVD and fast Fourier transform, which can accurately extract oscillation components that benefit from the adaptive threshold setting method. Second, the analysis center software is implemented based on identification results. By integrating the PMU calibrator in Part I with the analysis center in Part II, we can examine in depth the field PMU test applications in three test scenarios, including standard, playback, and field signal test. Results demonstrate the effectiveness and applicability of the proposed field PMU test methods from both Parts I and II.**

***Index Terms*—Phasor measurement unit (PMU), field test, signal identification, oscillation.**

I. Introduction

IMPROVEMENTS in the performance and data quality of the existing phasor measurement units (PMUs) require comprehensive field PMU test and calibration. The companion study (Part I) [1] for this paper presents a general framework consisting of a PMU calibrator and analysis center for field PMU test across multiple scenarios. In addition, synchrophasor and signal denoising methods are proposed to ensure the calibrator accuracy for complex field signals. Next, in this paper, we analyze the analysis center and present the applications for field PMU test.

The analysis center is a computer that receives measurement results and evaluates the performance of the field PMU. This includes three modules: signal identification, error analysis, and performance evaluation. The signal identification module uses synchrophasor measurement to identify the signal types, as the field PMU has different measurement performances for different signal types. The error analysis module obtains the measurement errors of the PMU under test (PUT) by comparing the estimation results of the PMU calibrator and the PUT. The performance evaluation module determines the error levels according to signal type and interference level.

Because the error analysis and performance evaluation modules can be realized with the ease based on PMU standards [2], they are not discussed here. Instead, we focus on the signal identification module.

The field signal types are unknown. Because different field signal types require distinct evaluation indicators, identifying that the signal types are necessary. According to PMU standards, static and dynamic signals can be divided into three types: frequency linear changing, distortion, and phasor nonlinear changing. The frequency linear changing signals include fixed frequency offset and frequency ramping signals, which can be easily identified by the estimated frequency. In Part I, the PMU calibrator calculates the interference content of the field signals, allowing the distortion signal to be determined. Thus, the signal identification module focuses on identifying nonlinear dynamic signals. Based on PMU standards and field signal analysis, typical nonlinear dynamic signals generally include step and modulation/oscillation signals.

The step and oscillation of signals are critical in the evaluation of field PMUs [3], [4]. The measurement results during the step process are meaningless, leading to an irrelevant error analysis. In addition, synchrophasor algorithms exhibit different measurement performances under different oscillation frequencies. Thus, distinct requirements must be employed to evaluate the PUT estimation errors. The signal recognition module of the proposed framework identifies the

Manuscript received: August 2, 2021; revised: November 18, 2021; accepted: March 22, 2022. Date of CrossCheck: March 22, 2022. Date of online publication: June 27, 2022.

This work was supported by the National Natural Science Foundation of China (No. 51725702).

S. Xu, H. Liu (corresponding author), and T. Bi are with the State Key Lab of Alternate Electric Power System with Renewable Energy Sources (North China Electric Power University), Beijing 102206, China, and S. Xu is also with State Grid Jangsu Electric Power CO., LTD Research Institute, Nanjing 211103, China (e-mail: 18515422011@163.com; hliu@ncepu.edu.cn; tsbi@ncepu.edu.cn).

DOI: 10.35833/MPCE.2021.000527

two nonlinear dynamic signal types.

The existing step signal detection and identification methods can be divided into three categories as follows.

1) The methods based on real [5] and complex [6] wavelets, which employ amplitude and phase information, respectively, to locate mutations. However, these methods are highly sensitive to noise and harmonics. In addition, they cannot determine whether the signal step is caused by the frequency components in the PMU measurement band or by harmonics and interharmonics.

2) The methods based on empirical mode decomposition (EMD) [7], local mean decomposition (LMD) [8], and variational mode decomposition (VMD) [9], which perform multiscale decomposition of power signals. Hilbert transform is then implemented to obtain the instantaneous frequency of each frequency component, thus locating the step time. However, these methods are limited by endpoint effects, whereas EMD and LMD exhibit mode aliasing. In addition, these methods have high-computational complexity and are sensitive to noise.

3) Discrete Fourier transform (DFT) [10] and S-transform (ST) [11]-[13], which estimate the fundamental amplitude of the field signal. The step signal is then detected based on the statistical characteristics of the amplitude, e. g., mean value and variance. However, the amplitude and phase angle are measured by the PMU or PMU calibrator. This means that employing the DFT or ST amplitude is unnecessary. In addition, the statistical characteristics of the amplitude cannot effectively reflect the features of depth steps of weak oscillation. Therefore, these methods are generally not used to detect multi-step signal types.

The existing oscillation/component signal identification methods mainly include fast Fourier transform (FFT) and its variants [14], Prony [15], [16], EMD [17], TLS-ESPRIT [18], and Taylor Fourier transform [19]. These methods focus on the extraction accuracy of the oscillation components while attempting to determine whether a frequency component is the random noise or an effective component is limited. In addition, some methods may have large calculational burdens and cannot be applied in real time. Oscillation signal identification does not require high accuracy. Thus, FFT is a better method for determining oscillation component parameters due to its low-computational burden and high-numerical stability. However, FFT analysis cannot easily determine whether a frequency component is an effective signal or noise. Therefore, a fixed threshold is commonly used to extract frequency components [14]. Yet, in a power system, different lines may exhibit distinct noise levels and oscillation component amplitudes, which means that it is difficult to apply a fixed threshold value for multiple scenarios. To avoid this, an adaptive threshold-setting method is proposed to extract frequency components [20]. However, this method is limited by the fact that it misses the detection instances for small-oscillation component amplitudes.

Therefore, the following novel signal identification methods are proposed in this paper to address the aforementioned problems.

1) Based on the energy leakage of the signal during the step process, a step signal detection method based on singular value decomposition (SVD) is proposed. This method can detect the weak steps of fundamental and oscillation components.

2) Considering the high resolution of SVD, an oscillation signal identification method based on SVD and FFT is developed. This method can adaptively set a threshold to separate oscillation components and random noises.

3) To verify the effectiveness of the proposed methods in Parts I and II, a test system that includes a PMU calibrator and analysis center is developed and applied to evaluate the performance of a field PMU in several test scenarios, including standard, playback, and field signal test.

The remainder of this paper is organized as follows. Section II presents the proposed detection and location method of the step signal. The identification method for the oscillation signal is presented in Section III. Section IV describes the implementation of the analysis center software. Applications of field PMU test and calibration platform are presented in Section V. Section VI concludes the study.

II. Detection and Location Method of Step Signal

A. Analysis of Requirements

The PMU measurement objects are the synchrophasors of the static and dynamic signals. Field PMU data analysis reveals the three-step signal types of field voltage signal in the power systems as shown in Fig. 1.

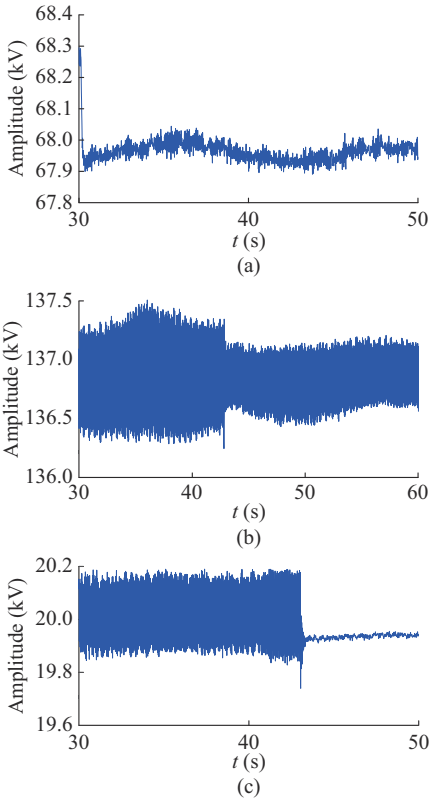

Fig. 1. Three-step signal types of field voltage signal. (a) Fundamental step. (b) Oscillation step. (c) Combined step.

1) Fundamental step: field signals do not have oscillation

components, and only the fundamental component mutates, which is the most common scenario in a power system. Figure 1(a) shows the amplitude of the field voltage signal, where the amplitude drops at 30 s from 68.3 kV to 67.9 kV (about 400 V, or 0.59%) at 30 s.

2) Oscillation step: field signals have oscillation components with a sudden change in oscillation depth. Figure 1(b) presents the measured amplitude of the field PMU during subsynchronous oscillation (SSO) with a 25-Hz oscillation frequency. The mean value of the phasor amplitude, i.e., fundamental amplitude, is maintained at approximately 136.8 kV, whereas the oscillation depth exhibits a sudden drop at 42 s from 500 V to 300 V (0.15%).

3) Combined step: both the fundamental and oscillation components exhibit sudden steps. Figure 1(c) demonstrates the voltage amplitude, where the fundamental amplitude changes from 20.0 kV to 19.9 kV and the oscillation component disappears at 43 s (0.50% and 0.75%, respectively, which correspond to the percentage of step size of fundamental and osciuation components).

A step detection method is required to identify the three-step signal types. Because the amplitude may be relatively small, the step detection method is also suitable for weak steps. In addition, the PMU test and calibration of the field signals have real-time requirements. Thus, the step detection method must have low computational complexity.

B. Proposed Step Detection Method

The existing methods are easily affected by interference components and cannot effectively detect the signal step for small sudden changes. Therefore, we propose a method based on SVD to detect and locate multi-step signal types. Because the synchrophasor can reflect sudden changes in both the amplitude and phase angle, it is used as the SVD object rather than as the amplitude or phase angle.

The step signal is caused by a sudden change in the main frequency components. Small-content components have a negligible influence on the mutation of the measurement results. During the mutation process and following the implementation of SVD, the fundamental and oscillation components exhibit energy leakages. This leaked energy has less effects on the singular values of large frequency components. However, it enhances the singular values of small components at the step time, as shown in Fig. 2. Therefore, determining the time-varying behavior of singular values enables the step signal to be identified.

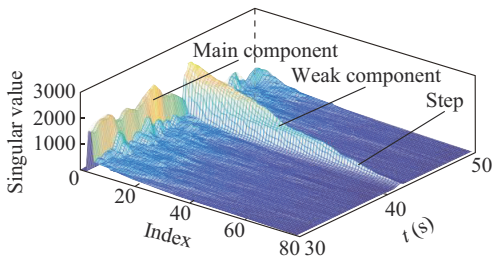

Fig. 2. Time-varying behavior of singular values at step time.

To obtain the singular values, we adopt the synchrophasor sequence to construct the Hankel matrix:

$$\boldsymbol{H}=\begin{bmatrix} \dot{\boldsymbol{X}}(1) & \dot{\boldsymbol{X}}(2) & \dots & \dot{\boldsymbol{X}}(C) \\ \dot{\boldsymbol{X}}(2) & \dot{\boldsymbol{X}}(3) & \dots & \dot{\boldsymbol{X}}(C+1) \\ \vdots & \vdots & & \vdots \\ \dot{\boldsymbol{X}}(L) & \dot{\boldsymbol{X}}(L+1) & \dots & \dot{\boldsymbol{X}}(N) \end{bmatrix}_{L\times C} \tag{1}$$

where $\boldsymbol{H}$ is the Hankel matrix obtained by mapping the one-dimensional synchrophasor sequence $\boldsymbol{X}(n)$ $(1\le n\le N)$ to a high-dimensional space; L is the number of matrix row; C is the number of matrix column; and $N=C+L-1$. When N is even, $L=N/2$; and when N is odd, $L=(N-1)/2$.

The singular values of $\boldsymbol{H}$ are then obtained by SVD:

$$\boldsymbol{H}=\boldsymbol{U}\boldsymbol{\Sigma}\boldsymbol{V}^{\mathrm{T}} \tag{2}$$

where $\boldsymbol{U}$ and $\boldsymbol{V}$ are the identity orthogonal matrices, which are the left and right singular matrices, respectively. Here, nondiagonal entries of $\boldsymbol{\Sigma}$ equal 0, and diagonal values are singular values:

$$\boldsymbol{\Sigma}=\begin{bmatrix} \sigma_1 & 0 & \dots & 0 \\ 0 & \sigma_2 & \dots & 0 \\ \vdots & \vdots & & \vdots \\ 0 & 0 & \dots & \sigma_L \end{bmatrix}_{L\times C} \tag{3}$$

where $\sigma_1,\sigma_2,\dots,\sigma_L$ are the singular values, and $\sigma_1>\sigma_2>\dots>\sigma_L$ indicate their arrangement from the largest to the smallest.

Note that the elements of $\boldsymbol{H}$ are complex, whereas singular values are real numbers. Each singular value corresponds to a frequency component, and its value is proportional to the amplitude of the frequency component. σ_1 is the fundamental component.

For the convenience of analysis, the singular values of $\boldsymbol{\Sigma}$ are extracted to construct the singular value spectrum $\boldsymbol{s}$:

$$\boldsymbol{s}=\mathrm{diag}(\boldsymbol{\Sigma}) \tag{4}$$

where $\boldsymbol{s}$ is a column vector of size $L\times 1$.

To obtain the time-varying curves of different singular values, we move to the next data window (ΔT denotes the time interval of two data windows) and use the new phasor sequence to obtain the new singular value spectrum.

Once K continuous singular value spectra are obtained, we construct a singular value spectral matrix $\boldsymbol{S}$:

$$\boldsymbol{S}=[\boldsymbol{s}_1 \quad \boldsymbol{s}_2 \quad \dots \quad \boldsymbol{s}_K]^{\mathrm{T}} \tag{5}$$

where $\boldsymbol{S}$ is composed of K continuous singular value spectra of size $K\times L$; and $\boldsymbol{S}(:,k)$ is the singular value of the k^{th} column with time-varying elements.

$\boldsymbol{S}(:,1)$ represents the time-varying curve of the singular value of the fundamental component, whereas $\boldsymbol{S}(:,2)$ to $\boldsymbol{S}(:,L)$ are the time-varying curves of the singular values of the remaining components. In general, the number of effective frequency components in the measurement band (0-100 Hz) is less than 10. Thus, $\boldsymbol{S}(:,11)$ to $\boldsymbol{S}(:,L)$ can be regarded as weak components and used to detect the step signal. However, the effect of energy leakage during the signal step on the singular values of the weak components decreases with the increase of k, as shown in Fig. 2. Multiple tests reveal that $\boldsymbol{S}(:,21)$ to $\boldsymbol{S}(:,L)$ are less affected by energy leakage of the step components. Thus, $\boldsymbol{S}(:,11)$ to $\boldsymbol{S}(:,20)$ are selected to detect the

synchrophasor step change.

C. Performance Verification

The window length of SVD data and the reporting rate of PMU calibrator are set to be 2 s and 100 Hz, respectively. In addition, as the time intervals of two data windows ΔT equal 0.1 s, the SVD is performed 10 times in 1 s (parameter selection is described in Supplementary Material A). The singular value of the 13rd column ($\boldsymbol{S}$(:,13)) is used to detect the step change of the synchrophasor.

For field signals, the amplitude and phase angle may be time-varying, and the fundamental frequency may deviate from the nominal frequency. In addition, the signal may be polluted by random noise. Thus, the simulation signal can be described as:

$$x(t)=50\sqrt{2}\,(1+0.01\varepsilon_{\mathrm{a}}(t))(1+0.1\cos(2\pi f_{\mathrm{m}}t))\cdot \cos\left(2\pi f_0 t+0.1\cos(2\pi f_{\mathrm{m}}t)+\frac{\pi}{180}\varepsilon_{\mathrm{p}}(t)\right)+noise \tag{6}$$

where f_{m} is the modulation frequency; f_0 is the fundamental frequency; and $\varepsilon_{\mathrm{a}}(t)$ and $\varepsilon_{\mathrm{p}}(t)$ are the unit step functions, which are defined as:

$$\begin{cases}\varepsilon_{\mathrm{a}}(t)=\begin{cases}0 & t<T_{\mathrm{a}}\\ 1 & t\geq T_{\mathrm{a}}\end{cases}\\ \varepsilon_{\mathrm{p}}(t)=\begin{cases}0 & t<T_{\mathrm{p}}\\ 1 & t\geq T_{\mathrm{p}}\end{cases}\end{cases} \tag{7}$$

where T_{a} and T_{p} are the time of the amplitude and phase step, respectively.

Subsequent test employs the following test parameters: test duration of 30 s; $f_0=50.1$ Hz; $f_{\mathrm{m}}=5$ Hz; the addition of 50 dB white Gaussian noise to test the signal; $T_{\mathrm{a}}=10$ s; $T_{\mathrm{p}}=20$ s; the amplitude step size of 1% of the fundamental amplitude; and the phase step size of 1°. Figure 3(a) presents the test signal, and Fig. 3(b) and (c) shows the amplitude and phase angle estimated by the synchrophasor algorithm proposed in Part I. The amplitude increases at 10 s. However, the location of the phase-angle step cannot be determined.

The proposed step detection method and disturbance identification method in [4] are used to analyze the estimated synchrophasor. The comparison method in [4] is based on the discrete wavelet transform (DWT), which is commonly used to localize discontinuities.

Step-detection results of proposed and compared methods are shown in Fig. 4. The singular values of the 1st column represent the fundamental component, where the amplitude step can be reflected. However, the phase step cannot be directly observed. The energy leakage results in a sharp increase in the singular value of the 13rd column at 10 and 20 s. This can be used to detect changes in the amplitude and phase angle step as well as the step time location. Level-1 and level-2 coefficients of the DWT-based method exhibit the same behavior as the amplitude shown in Fig. 3. However, this behavior is unhelpful for step detection because no singular point exists as in Fig. 4(a). Thus, the proposed method performs well in the detection of step signals under dynamic and noisy conditions.

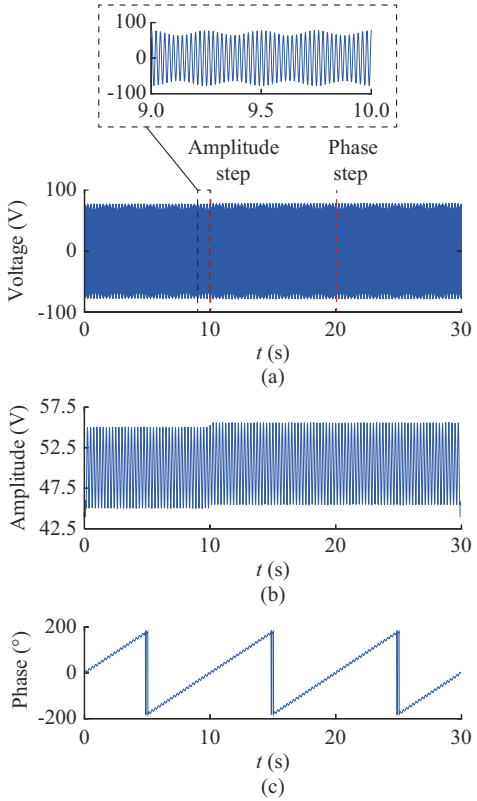

Fig. 3. Step signal waveform and estimated amplitude and phase angle. (a) Test signal waveform. (b) Amplitude. (c) Phase angle.

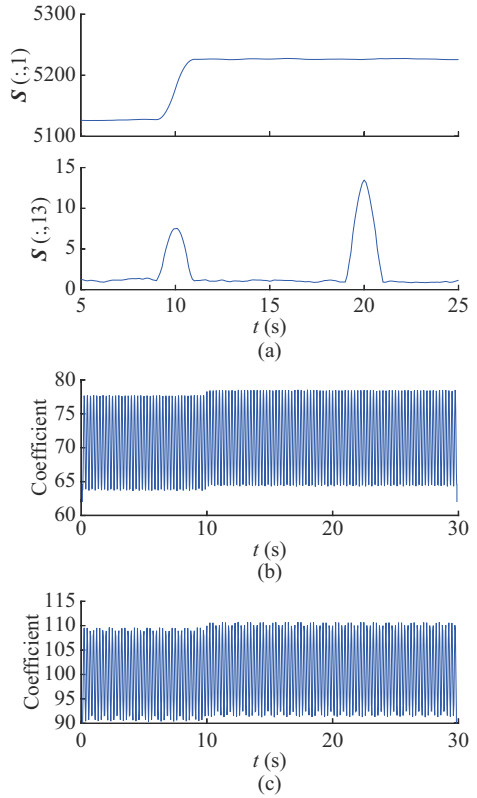

Fig. 4. Step-detection results of proposed and compared methods. (a) Time-varying curves of singular values of the 1st and 13rd columns. (b) Level-1 coefficients of DWT. (c) Level-2 coefficients of DWT.

III. Identification Method for Oscillation Signal

A. Analysis of Requirements

In power electronics enabled power systems, in addition to traditional low-frequency oscillations, SSOs induced by sub/supersynchronous interharmonics frequently occur [21]. Currently, PMUs are used for SSO monitoring [22], [23]. Therefore, the range of the oscillation signal identification extends from 45-55 Hz to 0-100 Hz.

PMU measurement errors generally increase with oscillation frequency. Thus, different oscillation frequencies should correspond to different error requirements. For example, the error requirements of an SSO should exceed those of low-frequency oscillations. Thus, we identify the oscillation parameters of the field dynamic signals, which provides a basis for PUT performance evaluation.

Theoretically, each oscillation frequency corresponds to an evaluation index. However, this can be cumbersome in practice. Following PMU test standards, the oscillation signal in the modulation frequency range of 0.1-5 Hz is associated with only a single evaluation indicator [1]. Therefore, a frequency band corresponds to an evaluation index instead of an oscillation frequency.

Currently, the maximum reporting rate is 100 Hz for a 50-Hz power system. Therefore, the maximum measurement band of the synchrophasor is 0-100 Hz. Following PMU test standards, we divide this range into 5-Hz intervals, where each 5-Hz frequency band corresponds to an evaluation index. For example, only one evaluation index is required for the 40-45 Hz oscillation components. Therefore, we extract only the dominant oscillation component in each frequency band without requiring high-identification accuracy for each component.

B. Proposed Identification Method

We next propose a method for identifying the oscillation components based on FFT and SVD. Because the synchrophasor contains the oscillation components of the amplitude and phase angle, the analytical object of the proposed identification method is also the measured synchrophasor of the PMU calibrator.

1) Identification Idea

To overcome the difficulties of FFT in distinguishing the effective frequency components from noise in real time, we use the SVD method to determine the threshold value of the amplitude spectrum. We take advantage of the following SVD capabilities: ① the SVD method is implemented in step detection, and thus no computational burden is added; ② SVD has a higher frequency resolution compared with FFT; and ③ the singular value of the oscillation component is proportional to its amplitude, as shown in Supplementary Material B:

$$A_{\mathrm{osc}} = \frac{\sigma_{\mathrm{osc}}}{R} \tag{8}$$

where A_{osc} and σ_{osc} are the amplitude and singular value of the oscillation component, respectively; and R is the ratio of the singular value to the amplitude, which is determined by the Hankel matrix dimension and window length of SVD data. Therefore, determining the SVD threshold value enables us to obtain the FFT threshold value.

Each singular value corresponds to a frequency component in the synchrophasor, and the singular value spectra are arranged from the largest to the smallest. Thus, the oscillation component with the larger amplitude must correspond to the previous singular value. Accordingly, a singular value threshold can be used to divide the effective and noise components:

$$\sigma_1 > \sigma_2 > \ldots > \sigma_{k-1} > \sigma_{th} > \sigma_k > \sigma_{k+1} > \ldots > \sigma_L \tag{9}$$

where σ_{th} is the singular value threshold; σ_1 - σ_{k-1} are the singular values of the effective components; and σ_k - σ_L are the singular values of the noise components. The FFT-determined threshold value of the amplitude spectrum A_{th} is then described as:

$$A_{th} = \frac{\sigma_{th}}{R} \tag{10}$$

2) Determination of Effective Order

To obtain the threshold, we must first determine the effective order of singular values. Most of the existing methods assume a mutation point between the singular values of the effective and noise components. Various approaches have been proposed to determine the mutation point of the singular-value spectrum, including the monotonously increasing function [24], relative difference [25], and median value [26] methods. However, the mutation point does not exist or cannot be easily located in complex field signals.

Accordingly, we consider singular values with a small proportion as random noise and obtain the singular values σ_1 - σ_L of the synchrophasor sequence using (4). Based on this, the ratio of a singular value to the sum of its subsequent singular values is determined as:

$$C_i = \frac{\sigma_i}{\sum_{k=i}^{L} \sigma_k} \times 100\% \tag{11}$$

The indicator in (11) avoids the influence of large singular values on subsequent singular values.

To determine the effective order using the indicator in (11), conducting a numerical analysis is required. We assume that the power signal is composed of the following six frequency components:

$$\begin{aligned} x(t) = {} & 50\sqrt{2}\cos\left(2\pi \times 50.7t + \frac{\pi}{3}\right) + 0.5\sqrt{2}\cos\left(2\pi \times 45t + \frac{\pi}{4}\right) + \\ & 5\sqrt{2}\cos\left(2\pi \times 47.3t + \frac{\pi}{5}\right) + 5\sqrt{2}\cos\left(2\pi \times 48.3t + \frac{\pi}{6}\right) + \\ & 0.5\sqrt{2}\cos\left(2\pi \times 52t + \frac{\pi}{5}\right) + 0.5\sqrt{2}\cos\left(2\pi \times 53t + \frac{\pi}{6}\right) + \\ & noise \end{aligned} \tag{12}$$

Figure 5(a) presents C_i under 30 dB of random noise. The first six ratios represent the effective components, where the subsequent ratios are random noise. The ratios of the effective components exceed those of the noise components.

Figure 5(b) shows the ratio fluctuations of the singular value of the 7th column C_7 following the addition of several ran-

dom noise levels, where C_7 is close to 10% at all noise levels. When the test signal contains several effective components, the first singular value ratio of the noise components remains close to 10% across different SNRs. Multiple tests indicate that singular values with ratios less than 10% should be considered as random noise.

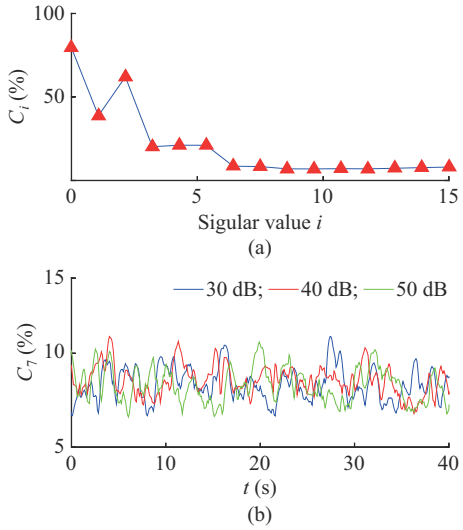

Fig. 5. Singular value ratios under 30 dB of random noise and the first singular value ratio of noise components under different noise levels. (a) C_i under 30 dB of random noise. (b) C_7 under different noise levels.

Note that when the effective component content is small, it may be fused with random noise. In this case, the singular value ratio of the effective component may be less than 10% and the effective component cannot be identified.

However, this does not affect the final PMU performance evaluation because the weak oscillation components have little effect on synchrophasor accuracy. In addition, each frequency band has only a single evaluation indicator. Thus, each indicator is only required to determine the dominant oscillation component in each frequency band rather than accurately locating each oscillation component. This means that none of the weak components need to be identified.

When C_k is less than 10%, the first k–1 singular values are the effective singular values, and the effective order is equal to k–1. The singular value spectrum threshold can be determined adaptively using the method previously described.

$$\sigma_{th}=\frac{\sigma_k+\sigma_{k-1}}{2} \tag{13}$$

3) Process of Oscillation Identification

Once the singular value spectrum threshold is obtained, we determine the relationship between the singular value and amplitude of the oscillation component. If the window length of SVD data and Hankel matrix dimension have been determined, the ratio of the singular value to the amplitude of a single frequency component is constant. In our experiments, we employ the window length of SVD data of 2 s and a Hankel matrix dimension of 101×100. Thus, the ratio of the singular value to the amplitude is approximately 142. In this case, the amplitude spectrum threshold can be obtained using (10).

In summary, the oscillation signal identification is performed according to the following steps.

1) The ratio R between the singular value and amplitude is calculated based on the SVD parameters.

2) FFT analysis and SVD are employed to obtain the amplitude and singular value spectra of the synchrophasor.

3) C_i is calculated using (11) to determine the threshold σ_{th} of the singular value spectrum. A_{th} of the amplitude spectrum is then obtained using (10).

4) The maximum amplitude of each frequency band is compared with A_{th}. FFT exhibits the fence effect, which can potentially lower the effective component altitudes to less than the threshold and which in turn requires that the maximum amplitude, e. g., the interpolation FFT method [17], should be corrected. The corrected amplitudes are compared with A_{th} to determine whether they are effective components.

C. Performance Verification

1) Simulation Test

The proposed method (threshold setting method A (SA)) is compared with the adaptive threshold setting method (threshold setting method B (SB)) proposed in [23]. The simulation signal model is described in (12) with a random noise 30 dB. The amplitude spectrum of the synchrophasor is shown in Fig. 6(a), where the threshold values of SA and SB are 0.3 A and 0.1 A, respectively. Both methods can identify the effective components and noise.

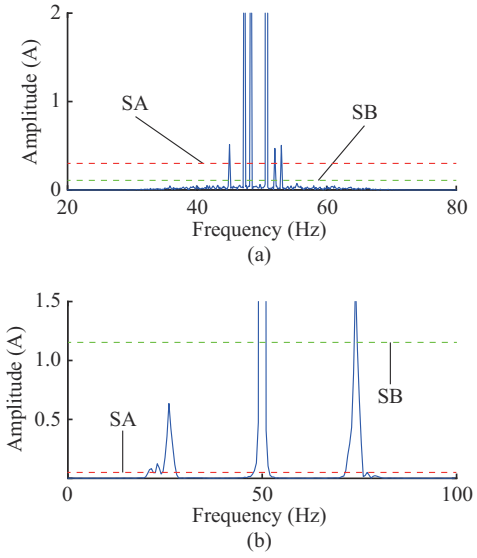

Fig. 6. Amplitude spectrum threshold values. (a) Simulation signal. (b) Field signal.

2) Field Data Test

The recorded current data of the SSO in the renewable area are analyzed. Field signals are shown in Fig. 6(b), where the threshold values of 0.05 A and 1.15 A are given for SA and SB, respectively. The SB cannot identify the oscillation component at 26 Hz, whereas the SA can identify the effective components, including those with a small amplitude (23 Hz in Fig. 6(b)). Therefore, the proposed method improves the identification effect as compared with the SB and can be

effectively applied to field signals.

IV. Implementation of Analysis Center Software

We integrate the analysis described in Section III with the PMU calibrator described in Part I to implement an LABVIEW-based analysis center. Through this integration, we calculate the measurement errors and herein present the test results. The analysis center, as shown in Supplementary Material C, can be divided into three areas as follows.

1) Area A is used to present the estimation results of the PUT and PMU calibrator, including the amplitude and phase angle of the voltage and current signals, frequency, and rate of change of frequency (ROCOF).

2) Area B presents the estimation errors over a certain period (e. g., 1 min) and their maximum values, mean deviation, and standard deviation.

3) Area C presents the identification results of the voltage and current signal types, including the step and oscillation signals. For the step signal, the step time and time-varying curve of the singular values are presented, whereas for the oscillation signal, the oscillation time, amplitude, and frequency are reported in tables.

V. Applications of Field PMU Test and Calibration Platform

In Part I, we introduce three field PMU test scenarios: standard, playback, and field signal test. Here, we present the PMU test results in these scenarios to demonstrate the effectiveness of the proposed test system including the PMU calibrator and analysis center in Parts I and II, respectively. In this section, standard, playback, and field signal tests are presented in Section V-A, V-B, V-C, respectively.

The recorded voltage and current waveforms are used as the field test signals. The waveforms of 1 min are recorded as a COMTRADE file at a sampling rate of 1200 Hz. Thus, the recorded field data under disturbances are used in the playback and field signal test. To ensure clarity, we present the test results in tables and figures rather than in the interface, as shown in Fig. C1 of Supplementary Material C.

A. Standard Signal Test

The test setup is shown in Supplementary Material C, where the generator sends the test signals specified in IEEE standards to the PUT and PMU calibrator [27]. The PUT performance is quantified by comparing PUT and calibrator measurements. The test results are listed in Table I, where OOB stands for out-of-band test, AM stands for amplitude modulation test, PM stands for phase modulation test, TVE stands for the total vector error, FE stands for the frequency error, and RFE stands for the ROCOF error. PUT can meet the standard accuracy requirements, where the errors can be one order of magnitude lower than the limitations in interference and modulation test. In addition, the phasor accuracy is five times higher than the standard requirements. Therefore, PUT can be used to estimate the synchrophasor in real power systems.

TABLE I
The Maximum Errors of PUT Under Static and Dynamic Conditions

Test type	TVE (%)		FE (Hz)		RFE (Hz/s)	
	IEEE	PUT	IEEE	PUT	IEEE	PUT
Off-nominal	1.0	0.109	0.005	0.00076	0.1	0.011
Harmonic	1.0	0.072	0.025	0.00043		
OOB	1.3	0.071	0.010	0.00049		
AM	3.0	0.091	0.300	0.00200	14.0	0.001
PM	3.0	0.113	0.300	0.00200	14.0	0.057
Frequency ramp	1.0	0.098	0.010	0.00200	0.2	0.053

B. Playback Signal Test

In this test scenario, the generator shown in Fig. C1 is used to play back the field-recorded waveform under disturbances. Figure 7 presents the playback waveform containing the harmonics and interharmonics (23 Hz and 77 Hz, respectively), where the fundamental amplitude is time-varying. As the reporting rate equals 50 Hz, PUT must reject the interharmonics.

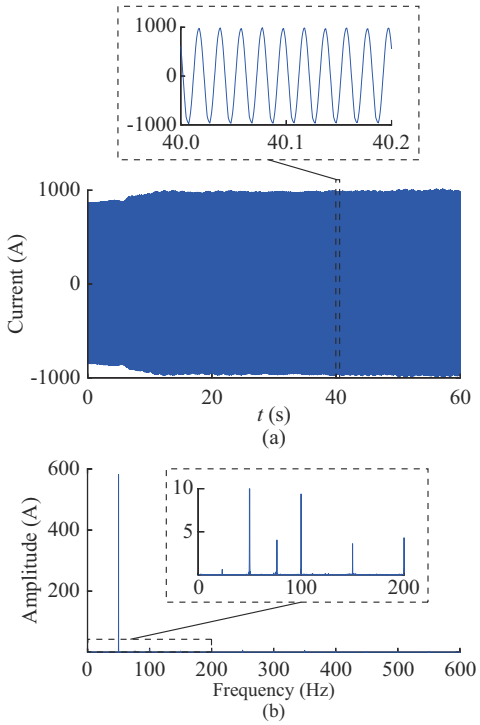

Fig. 7. Playback waveform and its spectrum. (a) Current waveform. (b) Current spectrum.

The current shown in Fig. 7 is then transformed into the secondary-side current for playback. Figure 8 shows the amplitudes measured by the PMU calibrator and PUT as well as the amplitude error (AE) of PUT. The amplitude does not oscillate with high frequency. Therefore, PUT can filter out the harmonics and interharmonics. In addition, the PUT can track the time-varying amplitude. However, it exhibits a slight attenuation effect on the high current amplitude. This results in an AE of 0.4%-0.6%, indicating that the parameters of this PMU require the calibration or adjustments.

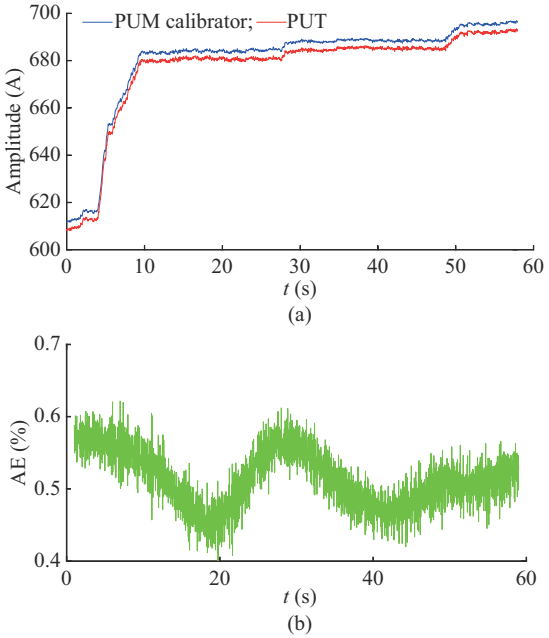

Fig. 8. Amplitudes measured by PMU calibrator and PUT as well as AE of PUT. (a) Amplitudes measured by PMU calibrator and PUT. (b) AE of PUT.

C. Field Signal Test

To test the field PMU in a substation, a corporation with related utilities is required. Thus, at this stage, the recorded and synchrophasor data of the field PMU are used to verify the performance of the test system in Scenario C. The PMU calibrator measures the synchrophasor of the recorded data to provide reference values. The phasor data of the PMU calibrator and PUT are then compared to evaluate the PUT performance. In this case, the field PMU is an M-class PMU with a reporting rate of 100 Hz.

The field PMU is deployed in a substation of a renewable area that exhibits complex field signals (noisy, step, SSO, etc.). Therefore, this test scenario requires the implementation of signal denoising and signal-type identification methods. It should be noted that these methods are evaluated by simulation tests in [1] and earlier in this study. To further verify their performances, these methods are tested using field data.

1) Denoising Method Test

The denoising method is proposed in Part I. Its parameter settings and denoising effects as compared with other denoising methods in simulation tests are also presented in Part I. Next, quasi-steady voltage and dynamic current signals are used to test the performance of the proposed denoising method under static and dynamic conditions, respectively.

1) Quasi-steady signals

The measurements of the PUT and PMU calibrator are shown in Fig. 9, where "noise" denotes the results of the field PMU, DA is the proposed method, and DC is the SVD-based denoising method (as shown in [1]) [28]. The DA and DC are implemented using the PMU calibrator. The field PMU does not use a denoising method. Therefore, its amplitude and frequency have many burrs and severe jitters, including 0.2-kV and 0.01-Hz jitters in amplitude and frequency, respectively. Following signal denoising, the amplitude and frequency determined from the DC still exhibit fluctuations, where those of DA are smoother (with 0.05-kV and 0.003-Hz jitters in amplitude and frequency, respectively). This indicates the improved ability of DA to denoise the field signals under a quasi-steady condition as compared with the DC, thus improving the estimation accuracy of the PMU calibrator.

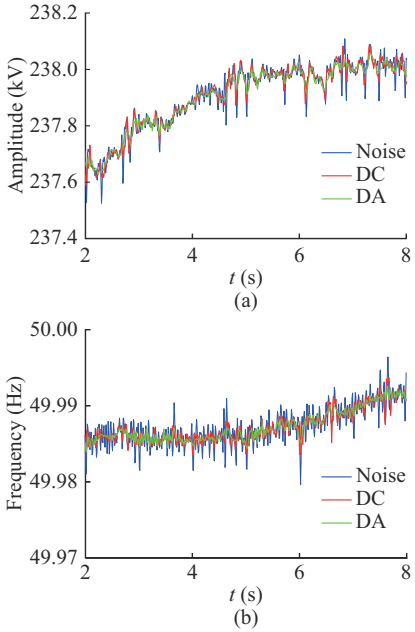

Fig. 9. Estimated amplitudes and frequencies of PUT and PMU calibrator with denoising method. (a) Amplitudes of original and denoised voltage signals. (b) Frequencies of original and denoised voltage signals.

2) Dynamic signals

The current signals in the renewable area may contain a high noise level, and SSO may also be present. The recorded current waveform is shown in Fig. 10, where the amplitude is modulated at 26 Hz.

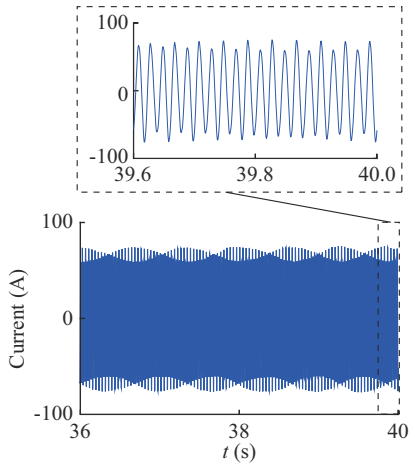

Fig. 10. Recorded current waveform in renewable area.

The estimated amplitudes are shown in Fig. 11. The amplitude of the current signal without denoising varies with time, and small fluctuations induced by random noise are

added to the dynamic amplitude. The DC method exerts a small denoising effect on the dynamic signals, with the denoised amplitude exhibiting small fluctuations. With the proposed method, the amplitude of the denoised signal shows the same behavior of the change as the original amplitude, but the fluctuations are considerably suppressed. As a result, the proposed method shows good performance for dynamic signals in real power systems.

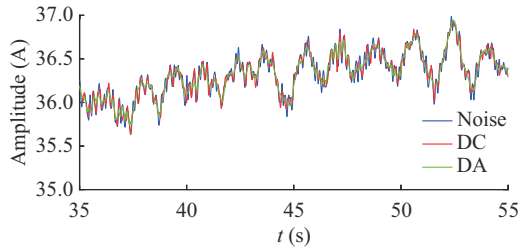

Fig. 11. Estimated amplitudes of original and denoised current signals in renewable area.

Thus, the simulation tests in Part I and field tests here in Part II fully verify the effectiveness of the proposed denoising method.

2) Test of Step Detection Method

The data measured by PMUs during the step or transient processes are meaningless, leading to invalid results.

This means that the results close to the step time should not be used to evaluate the performance of field PMUs and that locating the step time is required.

The proposed SVD-based method is used to monitor and locate the step time in real time. In Area C of Fig. A4 of Supplymentary Material A, the step time is recorded in tables, allowing the analytical results to be located close to the step time. The following two cases are considered to verify the effectiveness of the proposed method.

1) Large step size

Figure 12(a) presents the time-varying curve of the 13rd singular values over 1 min. The singular values at 43 s exhibit a sudden change, indicating a step time of 43 s. Then, the recorded field current waveform and estimated results of the PUT and PMU calibrator close to the step time are found, as shown in Fig. 12(b) and Fig. 13. According to the waveform and amplitude, the amplitude step is also 43 s, with a step size of approximately 13%. Thus, the proposed method can accurately locate the step time.

Although the AE at the step time reaches 4%, it cannot be considered as the maximum error of the field PMU. The evaluations of PMU performance require an error close to the step time to be neglected. At this time, the maximum AE is approximately 0.6% due to the occurrence of SSO. This indicates the necessity of step detection in PMU evaluation.

2) Small step size

The step time in Area C of Fig. A4 of Supplementary Material A reveals an additional amplitude step. Figure 14(a) shows the time-varying curve of the 13rd singular value, where the singular values change suddenly at 17.5 s, indicating the occurrence of an amplitude step.

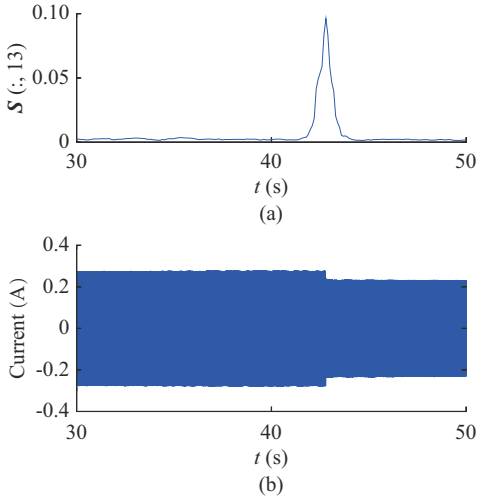

Fig. 12. Time-varying curve of the 13rd singular values in large step size of field signals and recorded field current waveform. (a) Singular value curve. (b) Field current waveform.

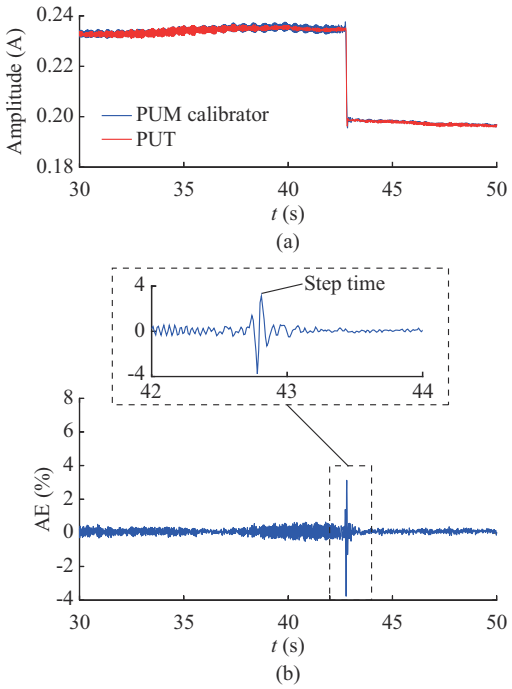

Fig. 13. Estimated amplitudes of PUT and PMU calibrator and AE of PUT close to step time for large step size. (a) Estimated amplitudes. (b) AE of PUT.

The waveform in Fig. 14(b) cannot reflect the amplitude step, but the estimated amplitudes of the PUT and PMU calibrator in Fig. 15(a) drop at 17.5 s. The amplitude step size is only 0.5%. Therefore, the proposed step detection method shows good performance in the weak step of field signals.

Figure 15(b) shows that the maximum AE close to the step time increases to 0.5%, but this is an invalid result. The maximum AE of the field PMU is approximately 0.1% (excluding errors close to the step time). This error can meet the application requirements [1]. In summary, the proposed method can detect and locate weak step signals and provide a reference for performance evaluation of PMUs.

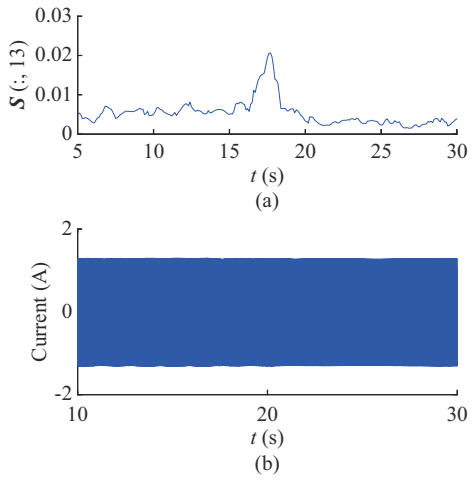

Fig. 14. Time-varying curve of the 13rd singular values for small step size of field signals and recorded field current waveform. (a) Singular value curve. (b) Field current waveform.

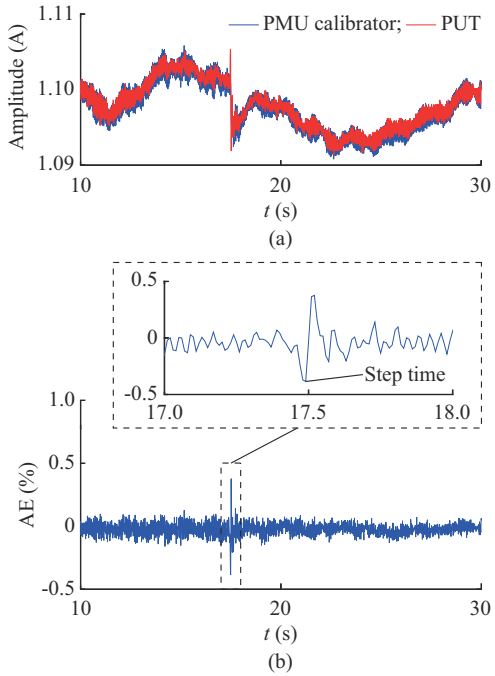

Fig. 15. Estimated amplitudes of PUT and PMU calibrator and AE of PUT close to step time for a small step size. (a) Estimated amplitudes. (b) AE of PUT.

3) Test of Oscillation Identification Method

Area C of Fig. A4 of Supplementary Material A shows the oscillation time, which can be used to locate the corresponding analytical results. A section of the oscillation signals is selected to verify the effectiveness of the proposed oscillation identification method.

The field current waveform during the oscillation time is shown in Fig. 16(a). FFT analysis reveals the field signal has sub/supersynchronous interharmonics of 31.5 Hz and 68.6 Hz, respectively, resulting in an SSO of approximately 18.5 Hz. The oscillation identification results are presented in Fig. 16(b), where the threshold obtained by the proposed method is 0.16 A. Thus, the oscillation components of 31 Hz and 69 Hz can be obtained, which are recorded in Fig. A4 of Supplementary Material A. This demonstrates the effectiveness of the proposed oscillation identification method for field oscillation signals.

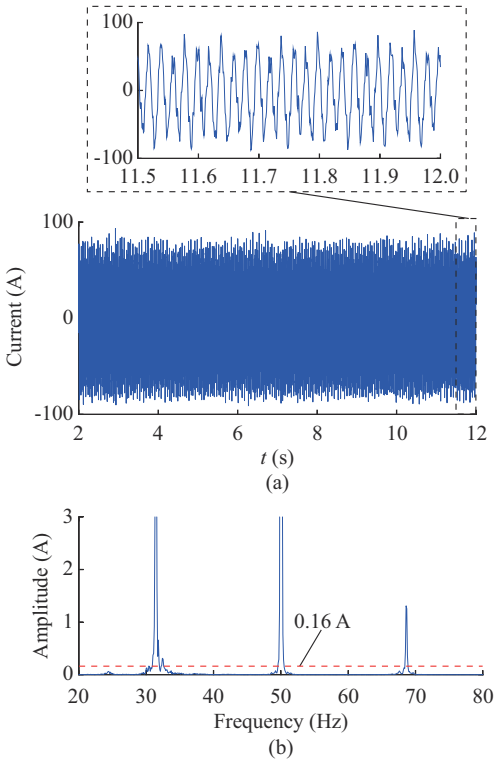

Fig. 16. Recorded field current waveform and oscillation identification results. (a) Field current waveform. (b) Oscillation identification results.

The measured amplitudes of the PUT and PMU calibrator are shown in Fig. 17. The field PMU is observed to suppress the SSO components, leading to an AE of 20%. To effectively monitor the SSO, the field PMU must be able to estimate the synchrophasors of high-frequency oscillations. Thus, the synchrophasor algorithm of the field PMU must be improved for efficient monitoring of the SSO. For excessive AEs, if the oscillation frequency is not given, it is not conducive to an objective performance evaluation of field PMUs.

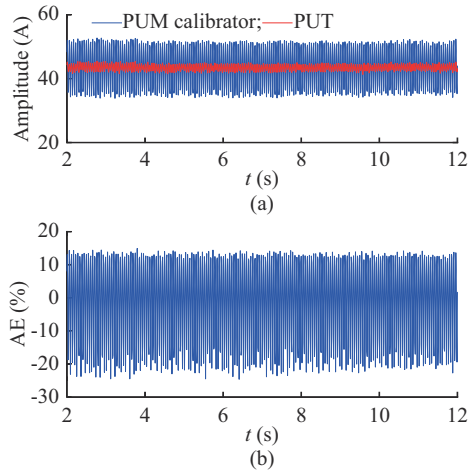

Fig. 17. Measured amplitudes of PUT and PMU calibrator and AE of PUT. (a) Measured amplitudes. (b) AE of PUT.

Therefore, the identification results shown in Fig. 16(b) can be used as a reference to evaluate the field PMU performance.

In summary, the proposed field test methods (including calibrator algorithms and signal identification methods) show good performance for complex field signals and thus can be used for field PMU test.

VI. Conclusion

In the second part of this two-paper set, the analysis center of the field PMU test system is analyzed. The signal identification module, which includes step detection and oscillation identification, is the focus of this paper. The identification results can provide an evaluation basis for field PMU error analysis. The analysis center software is implemented using the LABVIEW language and verified through standard, playback, and field signal test. The test results from Parts I and II reveal the effectiveness of the proposed test system based on the PMU calibrator, and its potential role in the field PMU test and calibration in multiple scenarios is highlighted.

Future work will focus on promoting the application of the proposed test system and improving its reliability. In addition, research work on the non-contact sampling of field current signals for test and calibration should be conducted to avoid the disconnection of field PMUs from power systems.

References

[1] S. Xu, H. Liu, and T. Bi, "Field PMU test and calibration method–part I: general framework and algorithms for PMU calibrator," *Journal of Modern Power Systems and Clean Energy*, vol. 10, no. 6, pp. 1507-1518, Nov. 2022.

[2] *IEEE/IEC International Standard - Measuring Relays and Protection Equipment–Part 118-1: Synchrophasor for Power Systems–Measurements*, IEC/IEEE 60255-118-1:2018, Dec. 2018.

[3] J. Ren and M. Kezunovic, "An adaptive phasor estimator for power system waveforms containing transients," *IEEE Transactions on Power Delivery*, vol. 27, no. 2, pp. 735-745, Apr. 2012.

[4] S. Vejdan, M. Sanaye-Pasand, and O. P. Malik, "Accurate dynamic phasor estimation based on the signal model under off-nominal frequency and oscillations," *IEEE Transactions on Smart Grid*, vol. 8, no. 2, pp. 708-719, Mar. 2017.

[5] I. Parvez, M. Aghili, A. I. Sarwat *et al*., "Online power quality disturbance detection by support vector machine in smart meter," *Journal of Modern Power Systems and Clean Energy*, vol. 7, no. 5, pp. 1328-1339, Sept. 2019.

[6] D. Zhang, Q. H. Wu, Z. Bo *et al*., "Transient positional protection of transmission lines using complex wavelets analysis," *IEEE Transactions on Power Delivery*, vol. 18, no. 3, pp. 705-710, Jul. 2003.

[7] S. Shukla, S. Mishra, and B. Singh, "Empirical-mode decomposition with hilbert transform for power-quality assessment," *IEEE Transactions on Power Delivery*, vol. 24, no. 4, pp. 2159-2165, Oct. 2009.

[8] X. Liu, J. Huang, Y. Yue *et al*., "Fault current identification of DC traction power supply system based on LMD time-frequency entropy," in *Proceedings of 2016 IEEE International Conference on Power and Renewable Energy (ICPRE)*, Shanghai, China, Oct. 2016, pp. 237-240.

[9] Y. Xu, Y. Gao, Z. Li *et al*., "Detection and classification of power quality disturbances in distribution networks based on VMD and DFA," *CSEE Journal of Power and Energy Systems*, vol. 6, no. 1, pp. 122-130, Mar. 2020.

[10] J. Burriel-Valencia, R. Puche-Panadero, J. Martinez-Roman *et al*., "Short-frequency fourier transform for fault diagnosis of induction machines working in transient regime," *IEEE Transactions on Instrumentation and Measurement*, vol. 66, no. 3, pp. 432-440, Mar. 2017.

[11] M. V. Chilukuri and P. K. Dash, "Multiresolution S-transform-based fuzzy recognition system for power quality events," *IEEE Transactions on Power Delivery*, vol. 19, no. 1, pp. 323-330, Jan. 2004.

[12] J. Li, Z. Teng, Q. Tang *et al*., "Detection and classification of power quality disturbances using double resolution S-transform and DAG-SVMs," *IEEE Transactions on Instrumentation and Measurement*, vol. 65, no. 10, pp. 2302-2312, Oct. 2016.

[13] W. Zhao, L. Shang, and J. Sun, "Power quality disturbance classification based on time-frequency domain multi-feature and decision tree," *Protection and Control of Modern Power Systems*, vol. 4, no. 27, pp. 1-6, Dec. 2019.

[14] H. Qian, R. Zhao, and T. Chen, "Interharmonics analysis based on interpolating windowed FFT algorithm," *IEEE Transactions on Power Delivery*, vol. 22, no. 2, pp. 1064-1069, Apr. 2007.

[15] D. Li, Y. Cao, and G. Wang, "Online identification of low-frequency oscillation in power system based on fuzzy filter and prony algorithm," in *Proceedings of 2006 International Conference on Power System Technology*, Chongqing, China, Oct. 2006, pp. 1-5.

[16] S. Ando, "Frequency-domain prony method for autoregressive model identification and sinusoidal parameter estimation," *IEEE Transactions on Signal Processing*, vol. 68, pp. 3461-3470, Jan. 2020.

[17] C. Shen, Z. An, X. Dai *et al*., "Measurement-based solution for low frequency oscillation analysis," *Journal of Modern Power Systems and Clean Energy*, vol. 4, no. 3, pp. 406-413, Jul. 2016.

[18] P. Tripathy, S. C. Srivastava, and S. N. Singh, "A modified TLS-ESPRIT-based method for low-frequency mode identification in power systems utilizing synchrophasor measurements," *IEEE Transactions on Power Systems*, vol. 26, no. 2, pp. 719-727, May 2011.

[19] L. Chen, W. Zhao, F. Wang *et al*., "An interharmonic phasor and frequency estimator for subsynchronous oscillation identification and monitoring," *IEEE Transactions on Instrumentation and Measurement*, vol. 68, no. 6, pp. 1714-1723, Jun. 2019.

[20] Z. Jin, H. Zhang, F. Shi *et al*., "A robust and adaptive detection scheme for interharmonics in active distribution network," *IEEE Transactions on Power Delivery*, vol. 33, no. 5, pp. 2524-2534, Oct. 2018.

[21] H. Liu, T. Bi, X. Chang *et al*., "Impacts of subsynchronous and supersynchronous frequency components on synchrophasor measurements," *Journal of Modern Power Systems and Clean Energy*, vol. 4, no. 3, pp. 362-369, Jun. 2016.

[22] F. Zhang, L. Cheng, W. Gao *et al*., "Synchrophasors-based identification for subsynchronous oscillations in power systems," *IEEE Transactions on Smart Grid*, vol. 10, no. 2, pp. 2224-2233, Mar. 2019.

[23] X. Yang, J. Zhang, X. Xie *et al*., "Interpolated DFT-based identification of sub-synchronous oscillation parameters using synchrophasor data," *IEEE Transactions on Smart Grid*, vol. 11, no. 3, pp. 2662-2675, May 2020.

[24] J. Xiao, X. Xie, Y. Han *et al*., "Dynamic tracking of low-frequency oscillations with improved Prony method in wide-area measurement system," in *Proceedings of IEEE PES General Meeting*, Denver, USA, Jun. 2004, pp. 1104-1109.

[25] S. K. Jain and S. N. Singh, "Exact model order ESPRIT technique for harmonics and interharmonics estimation," *IEEE Transactions on Instrumentation and Measurement*, vol. 61, no. 7, pp. 1915-1923, Jul. 2012.

[26] Y. Wang, Q. Li, F. Zhou *et al*., "A new method with Hilbert transform and slip-SVD-based noise-suppression algorithm for noisy power quality monitoring," *IEEE Transactions on Instrumentation and Measurement*, vol. 68, no. 4, pp. 987-1001, Apr. 2019.

[27] S. Xu, H. Liu, T. Bi *et al*., "A high-accuracy phasor estimation algorithm for PMU calibration and its hardware implementation," *IEEE Transactions on Smart Grid*, vol. 11, no. 4, pp. 3372-3383, Jul. 2020.

[28] S. Govindarajan, J. Subbaiah, A. Cavallini *et al*., "Partial discharge random noise removal using Hankel matrix-based fast singular value decomposition," *IEEE Transactions on Instrumentation and Measurement*, vol. 69, no. 7, pp. 4093-4102, Jul. 2020.

Sudi Xu is currently pursuing the Ph.D. degree in electrical engineering at North China Electric Power University, Beijing, China. His research interests include synchrophasor estimation and phasor measurement unit calibration techniques.

Hao Liu received the Ph.D. degree in electrical engineering from North China Electric Power University, Beijing, China, in 2015. He is currently an Associate Professor with North China Electric Power University. His research interests include synchronized measurement technique, test and calibration and their applications.

Tianshu Bi received the Ph.D. degree in electrical and electronic engineering from the University of Hong Kong, Hong Kong, China, in 2002. She is currently a Professor at North China Electric Power University, Beijing, China. Her research interests include power system protection and control, and synchrophasor measurement techniques and their applications.